Modeling and control of wave propagation in a ring with applications to power grids

Lea Sirota, *Member, IEEE*, and Anuradha M. Annaswamy, *Fellow, IEEE*

***Abstract*—This paper concerns the treatment of swing dynamics in a power grid using a continuous approach. Rather than addressing the problem as oscillations in a discrete system, we model the swing dynamics as a propagating electro-mechanical wave using a partial differential equation. A ring geometry with a one-dimensional wave equation is used to analyze the underlying dynamics. A control method is proposed to damp the system dynamics using the concept of Interior Wave Suppression. Unlike domains with boundaries such as strings, any concentrated input to the ring generates waves in two directions, thereby preventing total absorption. Using a judicious combination of concentrated control inputs, it is shown that a near uni-directional wave can be generated, with minimal back-waves. The resulting closed-loop system is proved to be stable. The overall modeling and control methods are shown to be implementable in a power grid using Phasor Measurement Units (PMU) as sensors and Flexible AC Transmission System (FACTS) devices, such as Thyristor Controlled Series Compensator (TCSC), as actuators. How the proposed methods of modeling and control can be applied to a network of rings is briefly discussed. Numerical simulations are carried out to validate the theoretical derivations.**

***Index Terms*—Swing oscillation damping, wave equation on a ring, uni-directional wave generation, wave suppression.**

I. Introduction

In a large power grid, where widely dispersed generators are interconnected through tielines, the essential characteristic that provides flawless power transmission through the network is synchronized swing of all generators. However, in the presence of disturbances, which may be caused due to any number of reasons including generation trips and outages or load changes, asynchronous motion can result. Such a motion leads to oscillations in the rotation frequency and angle resulting in increasing frequency swings, which are denoted by swing dynamics (see for example, [1], [2], [3], [4], [5]). Most of the existing approaches that deal with swing dynamics are based on spatially discrete modeling, implemented by ordinary differential equations (ODEs), and focus on analysis and synthesis using the ODE-models.

Our thesis, in contrast, is that when the number of generators is relatively large the fundamental mechanism that produces the phase and frequency oscillations is a continuous one. We claim that swing dynamics can be viewed as the electrical analogue of vibrations in a mechanical string. By this analogy, the generators constitute the inertia, the tieline admittance constitutes the string tension, and transmitting power over the grid is equivalent to sending a wave through the string. As a result, accurate and physically oriented methods for mitigating and suppressing these oscillations are better realized through the use of partial differential equations (PDEs). In this paper, we use a continuous approach for modeling and control of the swing dynamics in a power grid by treating it as a wave with a focus on a ring topology.

It should be noted that the problem of modeling the swing dynamics as a continuum has been examined by several researchers, see for example [6], [7], [8], [9]. In [6], the swing dynamics of a string of generators was modeled, for the first time, by an undamped wave equation. PDE modeling of more complex grid configurations including two-dimensional topology and various losses was carried out in [7] and [8], where inclusion of wind penetration was considered in [9]. Control of the continuously modeled swing dynamics was considered in [10], [11], [12]. In [10], optimal control algorithm was designed for the exact one-dimensional PDE. In [11], boundary controllers were designed for one and two dimensional lossless grids, which eliminated wave reflection from the boundaries. In [12], adaptive control of a continuously modeled string grid was designed using finite eigenmode discretization of the PDE. Existence and propagation of electro-mechanical waves through the grid was also observed in a high-fidelity simulation study undertaken in [13]. In particular, a series of videos showing FNET simulations on how electro-mechanical waves travel from New York to Florida in response to disturbances occurring in Tennessee can be found in [14].

The main distinction between the problem addressed in this paper and those above is that we consider a continuous system in the form of a ring. Rather than use a two-dimensional approach as in [7] and [8], where the two-dimensional wave equation was employed, we regard the grid as interconnected rings of generators with no boundaries present, where each ring is governed by the one-dimensional wave equation. Very few results have been reported in the literature, to our knowledge, on modeling and control of a continuous system with a ring topology. The second contribution of our paper is the control of the waves using the Interior Wave Suppression approach.

Control of systems governed by the wave equation, [15], is extensively discussed in the literature, proposing various methods to stabilize, regulate and track the system, e.g. [16], [17], [18], [19], to name a few. Here too, the focus of most papers has been on a string topology rather than a ring. The lack of a boundary in a ring introduces a significant challenge, as boundary control and related advantages of total wave absorption cannot be directly applied anymore. The main idea in a boundary control of waves in a string is the generation of

L. Sirota and A. M. Annaswamy are with the Department of Mechanical Engineering, Massachusetts Institute of Technology, Cambridge, MA, 02139 USA e-mail: {lbeilkin,aanna}@mit.edu.

a wave traveling in a single direction. The control strategy can then be viewed as an absolute absorption of waves incoming into the actuated end, thus preventing their further reflections (see for example, [18]). Such an approach is not applicable for rings, as any concentrated actuation is inherently interior, which in turn implies the generation of two waves traveling in opposite directions.

The proposed control method overcomes this challenge by utilizing a transfer function (TF) representation, a breakdown of the underlying disturbance waves into progressive and regressive components, and a generation of near-unidirectional control waves that cancel each of these components. By doing so, we are able to utilize the exact PDE-structure and accommodate the presence of damping, despite the latter introducing fractional order into the overall TF, similar to [20] and [21]. The presence of damping, however, is inevitable and has to be accommodated. Additionally, the presence of damping aids the stability of the overall system. The underlying control approach, denoted as Interior Wave Suppression (IWS), is inspired by that proposed in [22], [23], designed to control vibrations of continuous mechanical flexible structures. While a total wave suppression cannot be expected in a ring topology, we are able to achieve a significant suppression using the proposed control method. While much of the discussion of modeling and control is focused on a single ring topology, we briefly discuss as to how the approach can be applied to a network of rings.

The paper also discusses how the proposed IWS controller can be implemented and actuated in a power grid through the currently available Flexible AC Transmission System (FACTS) control devices such as the Thyristor Controlled Series Compensator (TCSC) and sensors such as Phasor Measurement Units (PMU) [1], [24], [25].

Preliminary results for both modeling and control using IWS were presented in [26], with a discussion of both string and ring topologies. However, in both cases, no damping was modeled. In this paper, we explicitly include damping in the underlying model while ensuring that the approach remains tractable despite the introduction of fractional order. The corresponding IWS controller differs from that in [26], and is simpler.

The paper is organized as follows. In Sec. II we derive the continuous TF model for the swing dynamics in a ring topology. In Sec. III we present the IWS control approach, specifically the near uni-directional wave generation mechanism and the controller design for a single ring (with a potential extension to multiple connected rings). In Sec. IV we discuss the implementation of the associated controllers in an actual power grid. In Sec. V we prove the resulting closed loop system stability and in Sec. VI we conclude the work.

II. Problem Statement: Continuous Model of Wave Propagation in a Ring

We consider the problem of disturbance regulation for the linear damped wave equation [15],

$$y_{tt}(u,t)+\beta y_t(u,t)=c^2 y_{uu}(u,t)+\tfrac{1}{\rho}\psi(u,t), \qquad (1)$$

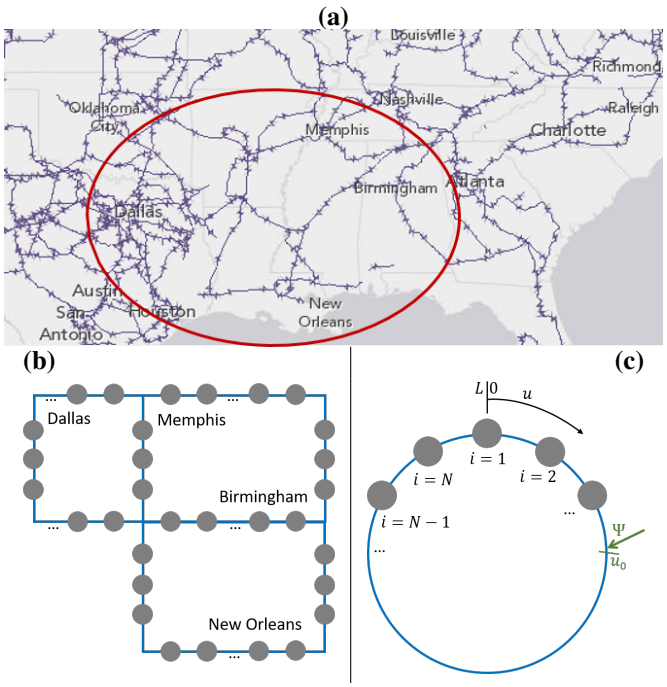

Fig. 1. **(a)** Part of the US west coast power network topology with major generators denoted by $*$. **(b)** The corresponding ring network representation of the grid in (a). **(c)** A single ring link with a disturbance $\Psi(t)$ acting $u=u_0$ and output measured at $u=u_m$.

on a closed string domain $u\in[0,L]$, which we denote by a ring of length L. Lowercase letters denote partial derivatives and $t\geqslant 0$ is time. Continuity of y and y_u at any point along the ring yields the end conditions $y(0,t)=y(L,t)$, and $y_u(0,t)=y_u(L,t)$. $c=\sqrt{T/\rho}$ is the propagation speed of the wave head, and T and ρ are, respectively, the equivalent string tension and the linear density. β is a normalized damping coefficient. We consider a disturbance $\psi(u,t)$ that penetrates the ring at a point u_0, i.e. it is a concentrated disturbance formally denoted by $\psi(u,t)=\Psi(t)\widehat{\delta}(u-u_0)$, where $\widehat{\delta}(\cdot)$ is Dirac's delta function.

As was discussed in Sec. I, a possible wave phenomenon in closed $1D$ domains is the swing oscillations in power grids, suggesting that these oscillations could be damped using the wave control method presented in this paper. Since the swing dynamics is commonly modeled as spatially discrete, we show in Section II-A that these discrete models coincide with the wave equation in (1) as the number of discrete elements increases, [6]. Simulation results are presented to corroborate this statement. In Section II-B, we derive the associated TF model, which in turn sets the stage for the control design proposed in Sec. III-B.

A. Spatially continuous model of power grid swing dynamics

Figure 1-(a) illustrates the major portion of the US power grid, with asterisks labeling the main generators. We regard the network as a collection of interconnected $1D$ closed-ended chains of generators, which we denote by rings. For example, the encircled area in Fig. 1-(a) accounts for three major rings between Dallas, Memphis, Birmingham and New Orleans, schematically outlined in Fig. 1-(b). In a single ring element comprising N generators (Fig. 1-c) the swing dynamics of

the i_{th} generator, $i \in [1,N]$, is usually described by a spatially discrete model, given by (see, e.g. [27])

$$\frac{2H_iS_i}{\Omega}\ddot{\delta}_i + B_i\dot{\delta}_i = P_i^M - P_i^E = P_i^M - \sum_{k=i-1,i+1}\frac{E_iE_k}{X_{i,k}}\sin(\delta_i - \delta_k). \tag{2}$$

Here $\dot{\delta}_i(t) = \omega_i(t)$ is the swing frequency of the i_{th} generator, $\Omega = 60_{[Hz]}$ is the base frequency, $H_{i[s]}$ is the inertia constant, $S_{i[MW]}$ is the generation rating. $P^M_{i[MW]}$ and $P^E_{i[MW]}$ are the mechanical and electrical power, respectively. $X_{i,k[MW^{-1}]}$ is the normalized reactance of the line segment $\{i,k\}$ and $E_{i[p.u.]} = 1$ is the normalized voltage amplitude. The damping B_i represents system losses augmented with secondary control, which keeps zero steady state swing frequency error, [28]. For small swing oscillations the model can be linearized about the equilibrium frequency Ω and equilibrium phases $\delta_i^* = \Omega t + \overline{\delta}_i$, where $\overline{\delta}_i$ is the initial phase shift. We then define the deviation swing frequency and angle by $\dot{y}_i(t) = v_i(t) = \omega_i(t) - \Omega$ and $y_i(t) = \delta_i(t) - \delta_i^*$. Assuming equal characteristics H,S,B for all the generators and equal spacing between them implying $X_{i,k} = X$, the linearized model becomes

$$\frac{2HS}{\Omega}\ddot{y}_i + B\dot{y}_i = \widetilde{P}_i^M + \frac{1}{X}(y_{i+1} - 2y_i + y_{i-1}). \tag{3}$$

To obtain the continuous representation of (2), we set the locations $i-1$, i and $i+i$ in (3) as $u-\varepsilon$, u and $u+\varepsilon$, respectively, where $\varepsilon = L/N$. Letting $\varepsilon \to 0$, (3) takes the form of the damped wave equation (1) with $T = \frac{1}{x}$ and $\rho = \frac{2Hs}{\Omega}$, where $s = \frac{1}{\varepsilon}S$ and $x = \frac{1}{\varepsilon}X$ represent generation and reactance densities, respectively. The electro-mechanical wave head propagation velocity c is then given by $c = \sqrt{\frac{T}{\rho}} = \sqrt{\frac{\Omega\varepsilon^2}{2HSX}}$. The distributed electrical power flow is then given by $\overline{p}^E(u,t) = \frac{1}{x(u)}y_u(u,t)$. The continuous limit of (3) then actually resembles the continuous model of the swing dynamics originally derived (for negligible damping) in [6]. The external disturbance $\psi(u,t)$ corresponds, for instance, to a spatially distributed deviation in mechanical power per unit length, $\widetilde{p}^M(u,t)$.

We stress that the mathematical limit $\varepsilon \to 0$ by no means implies a real zero distance between adjacent generators. As we demonstrate in Example 2.1, even for few dozens of kilometers the response of the discrete model (3) obeys traveling wave behavior predicted by the continuous system in (1).

Example 2.1: Adopting realistic power grid values suggested in [6], we consider a ring of length $L = 6400_{[km]}$ with $N = 200$ evenly spanned generators, characterized by $H = 5_{[s]}$ and $S = 375_{[MW]}$, with total line reactance of $X_{tot} = 0.0031_{[MW^{-1}]}$. The resulting parameters of the equivalent continuous model, (1), are wave propagation speed $c = 2577_{km/s}$ and characteristic time constant $\tau \approx 2.5_s$. The damping constant B was set to zero. A vanishing pulse disturbance $\Psi(t) = 0.1S\sin\frac{5\pi t}{\tau}e^{-t}[U(t) - U(t-0.4\tau)]$, where $U(\cdot)$ is the Heaviside function, penetrates the grid at $u_0 = \frac{1}{2}L$.
Time responses of swing frequency of the 150_{th} generator ($u_m = \frac{3}{4}L$) for both discrete and continuous models (3) and (1) are plotted in Fig. 2-(a). The two graphs overlap quite well, which demonstrates that the underlying swing dynamics can be represented effectively by a spatially continuous system. The response of the entire ring to the same disturbance is plotted in Fig. 2-(b). It shows that the concentrated pulse generates two electro-mechanical waves that propagate to the left and right repeatedly, confirming that the oscillations observed in Fig. 2-(a) are only a local effect of the overall wave phenomenon.

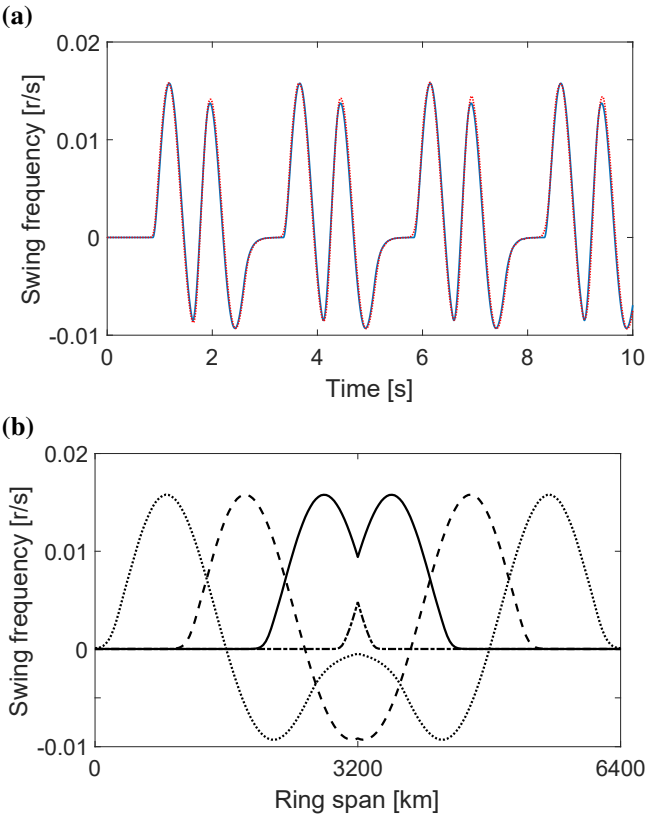

Fig. 2. Response of the swing frequency deviation $v(u,t)$ to a concentrated pulse disturbance in Example 2.1. **(a)** The response is plotted at $u = 0.85L$ and appears in the form of oscillations. Solid blue - simulation of the continuous model (1). Dotted red - simulation of the discrete model (3). **(b)** The response of the entire ring is plotted at four different time instances, $t_1 = 0.05\tau$ (dashed-dotted), $t_2 = 0.2\tau$ (solid), $t_3 = 0.35\tau$ (dashed) and $t_4 = 0.5\tau$ (dotted). Two traveling waves, a progressive and a regressive one, are generated.

B. Transfer function representation

Applying Laplace transform to (1) and the continuity conditions with respect to time (assuming zero initial conditions), and using, for convenience, the same notations for the transformed variables, gives a second order ODE in u,

$$\left(\frac{\lambda(s)}{c}\right)^2 y(u;s) = y_{uu}(u;s) + \frac{1}{T}\Psi(s)\widehat{\delta}(u-u_0), \tag{4}$$

where

$$\lambda(s) = \left(s^2 + \beta s\right)^{\frac{1}{2}}. \tag{5}$$

Assuming that the variable of interest is $v(u;s) = sy(u;s)$ (e.g. swing frequency in power grids), we obtain

$$v(u;s) = G_v(u,u_0;s)\Psi(s), \tag{6}$$

where $G_v(u,u_0;s)$ is the system Green's function or the TF from a concentrated input at u_0 to the output at u, given by

$$G_v(u,u_0;s)=\frac{1}{2\phi}\frac{s}{\lambda(s)\Delta(s)}\left[e^{-|\tau_u-\tau_{u_0}|\lambda(s)}+e^{-(\tau-|\tau_u-\tau_{u_0}|)\lambda(s)}\right], \tag{7}$$

where

$$\Delta(s)=1-e^{-\tau\lambda(s)} \tag{8}$$

is the characteristic equation (excluding $\lambda(s)$). The constant

$$\phi=\frac{T}{c} \tag{9}$$

is the undamped system's characteristic impedance, and

$$\tau=\frac{L}{c},\qquad \tau_u=\frac{u}{c},\qquad \tau_{u_0}=\frac{u_0}{c}, \tag{10}$$

are time constants. The absolute values in (7) indicate the relative location of the input at u_0 and the output at u. It can be seen that TF (7) is irrational and for $\beta>0$ it is of fractional order. The analogue of (7) for an open-ended string topology was discussed at length in [21] in the context of boundary control of the damped wave equation. Since (7) is infinite dimensional in Laplace domain, it accounts for the conjoint action of all vibrational modes, which indicates traveling wave phenomenon.

1) Progressive and regressive waves: In order to motivate the choice of control architecture that will be used to suppress the waves exhibited in (1), it is useful to further analyze the TF model in (7), which is carried out below.

It is well known that any input to a system governed by a linear wave equation generates two waves, equal in amplitude (both absolute value and sign) propagating in opposite direction with respect to each other, whether or not any damping is present. This is usually discussed in a string topology, with regard to effect of reflection from the boundaries [29], [30]. In a ring topology, one wave propagates clockwise and denoted by a progressive wave, whereas the other propagates counterclockwise and denoted by a regressive wave. These waves are captured by the infinite series expansion of (7), given by

$$G_v(u,u_0;s)=\frac{1}{2\phi}\frac{s}{\lambda(s)}\sum_{k=0}^{\infty}\left[e^{-\theta_1(u,k)\lambda(s)}+e^{-\theta_2(u,k)\lambda(s)}\right], \tag{11}$$

where the summation index k indicates a cycle of motion. The time that takes each wave generated at u_0 to reach u at the k cycle is given respectively by

$$\theta_1(u,k)=k\tau+|\tau_u-\tau_{u_0}|,\quad \theta_2(u,k)=(k+1)\tau-|\tau_u-\tau_{u_0}|. \tag{12}$$

For $\tau_u>\tau_{u_0}$, $\theta_1(u,k)$ stands for the progressive wave and $\theta_2(u,k)$ for the regressive, whereas for $\tau_u<\tau_{u_0}$ they are swapped. The two waves routes are illustrated in Fig. 3 for $\tau_u>\tau_{u_0}$ for the first cycle of motion ($k=0$ in (11)) with the arrival times (12) indicated above the arrows. The evolution of the wave shape during its propagation is determined by $\lambda(s)$, which is defined in (5). To obtain the time domain interpretation of (11), we denote each term of the series therein by $s\Gamma(\theta;s)$, where

$$\Gamma(\theta;s)=\frac{1}{\lambda(s)}e^{-\theta\lambda(s)}, \tag{13}$$

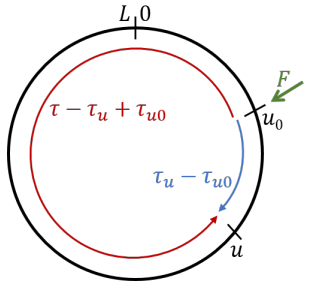

Fig. 3. The two routes a wave generated by a concentrated power input F at $u=u_0$ travel along the ring to the location u. The arrows indicate directions with the arrival times specified above each arrow. Blue - the progressive wave. Red - the regressive wave.

and θ represents any of the particular exponent arguments in (12). We then use the tables in [31] to calculate the inverse Laplace transform of (13), which is given by

$$\gamma(\theta,t)=e^{-\frac{1}{2}\beta t}I_0\left(\tfrac{1}{2}\beta\sqrt{t^2-\theta^2}\right)U(t-\theta). \tag{14}$$

The function $I_0(\cdot)$ is the zero order modified Bessel function of the first kind, [32]. The Heaviside function $U(\cdot)$ indicates that (14) is delayed by $t=\theta$. Since the wave head propagation speed c is independent of the damping coefficient β, the delay in (14) (or, equivalently, the wave arrival time) is independent of it as well. The speed of all the wave points except the head does depend on β (aka dispersion), which is expressed through the wave shape distortion during motion. The distortion is according to a convolution of the input with a shifted time derivative of (14).

For $\beta=0$, the damped wave equation (1) reduces to the classical wave equation. The fractional order terms $\lambda(s)$ are then reduced to s, indicating pure delay exponents in (11). Equivalently, the Bessel function in (14) then reduces to a delayed unity constant, implying that the output $v(u,t)$ is simply the shift of the input.

We conclude this section by discussing the stability of the open loop system (7). For $\beta=0$ the system is not stable. The poles of (7) are then given by $p_i=\frac{n\pi i}{2\tau}$, $n\in\mathbb{Z}$, which are the roots of $\Delta(s)$ in (8). All poles lie on the imaginary axis including one at the origin. For $\beta>0$ the system (7) becomes stable, which is rigorously proved in Sec. V. This can be motivated by the fact that $\frac{1}{\Delta(s)}$ changes to $\frac{s}{\lambda(s)\Delta(s)}$, which eliminates the pole at the origin and shifts the rest of the poles, in the presence of a nonzero β, to the open left half plane, which asymptotically approach the vertical line $-\frac{1}{2}\beta$.

In this section we showed that swing oscillations, an important problem in power grids, can be represented by a continuous model that describes wave propagation. We derived the model in time-domain, which coincides with (1), and its frequency domain counterpart in form of an infinite dimensional TF, (7). This TF model is valid for ring topology and is effective whether or not the system has damping.

The focus of the next section is on the design of a controller for wave suppression in the system. In the context of a power grid, it corresponds to the damping of swing oscillations (i.e. $y_t(t)\to 0$ as $t\to\infty$), thereby restoring equilibrium electrical power flow ($y_u\to const.$).

III. Interior Wave Suppression (IWS) Control

To achieve the wave suppression goal we carry out model-based control with the TF (7) as the starting point. Our control method is inspired by the AVS approach from [22], [23], [20], [21]. However, since the AVS method was designed exclusively for topology with boundaries, we cannot apply it to our ring system. We therefore develop a new approach, which achieves wave suppression by interior actuation.

When a $1D$ topology has boundaries (here an open ended chain, or a string), the two waves created by an input at the boundary are degenerated to a single wave traveling outward. Controlling the system through its boundary is therefore feasible, as the control wave can be uniquely designed to mitigate disturbances and achieve desired dynamics. For example, in [21] and [20] a boundary control wave is shaped in closed loop to cancel out reflected disturbance waves, attributed also to boundary impedance matching.

This control methodology, however, cannot be readily applied to a closed $1D$ topology without boundaries (the ring in Fig. 1-c). The intuitive explanation is that since a concentrated input at any location generates two waves, even if one of them, say, a forward wave, is designed to cancel out a disturbance wave, there will always remain the other wave, a back action wave or a back-wave, repeatedly circulating through the ring and constituting a disturbance of its own. In fact, the unavoidable back-wave elaborates on the general complexity associated with the inability to completely absorb waves through an interior point control, whether on a string or a ring, as was studied e.g. in [33], [34] and [35].

Our approach is based on minimizing the back-wave, while designing the forward wave to suppress the disturbance. To achieve this we propose a method to generate an interior, near uni-directional wave, using two concentrated actuators. A method to generate such a wave was originally proposed by the authors in [36] for an infinite line topology governed by the undamped wave equation ($\beta = 0$ in (1)). Based on this preliminary result, we derive in Sec. III-A a near uni-directional wave for a damped medium ($\beta > 0$ in (1)). We then use this wave as a control to cancel out disturbance propagation in (6). To make the concept clear, we first present the method for an undamped medium, which is then followed by the damped case.

A. Near uni-directional wave generation

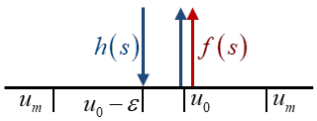

Fig. 4. Sample force diagram for generation of a near uni-directional wave on an infinite line. A signal f is applied at $u = u_0$ and a signal h is applied at $u = u_0$ and $u = u_0 - \varepsilon$ with opposite signs.

We carry out the derivation of the near uni-directional wave on an abstract infinite line topology. This was assumed here in order to present the idea of the directionality concept without involving the circulation effects of the ring topology. Suppose that there are two concentrated actuator inputs $f(t)$ and $h(t)$ on a section of an infinite line, as depicted in Fig. 4. $f(t)$ is acting at a single point $u = u_0$ and $h(t)$ is acting at two points $u = u_0$ and $u = u_0 - \varepsilon$, with equal magnitudes and opposite signs. We first consider the undamped case of $\beta = 0$. The transformed wave equation (4) then takes the form

$$\begin{aligned}\left(\tfrac{s}{c}\right)^2 y(u;s) = y_{uu}(u;s) + \tfrac{1}{T}\left[f(s)+h(s)\right]\widehat{\delta}(u-u_0) \\ - \tfrac{1}{T}h(s)\widehat{\delta}(u-(u_0-\varepsilon)).\end{aligned} \tag{15}$$

Using (6) and (7) with $u_0 = 0$ for brevity, the resulting velocity response to the combined action of both inputs can be represented in the frequency domain as

$$v(u_m;s) = \frac{1}{2\phi}e^{-\tau_{u_m}s}\cdot\begin{cases} f(s)+(1-e^{-\tau_\varepsilon s})h(s), & u_m \geq 0, \\ f(s)+(1-e^{+\tau_\varepsilon s})h(s), & u_m \leq -\varepsilon, \end{cases} \tag{16}$$

where the time constants are given by $\tau_{u_m} = \frac{u_m}{c}$ and $\tau_\varepsilon = \frac{\varepsilon}{c}$ and the response at $-\varepsilon < u_m < 0$ is not of interest. The central idea behind the near unidirectional wave generation can now be explained as follows. Suppose that the two control inputs are related as

$$h(s) = G_{h0}(s)f(s), \quad G_{h0}(s) = \frac{1}{\tau_\varepsilon(s+\eta)}, \tag{17}$$

where $\eta > 0$ is a design parameter that guarantees stable $G_{h0}(s)$. One can view the two-point actuation of $h(t)$ as a spatial differentiation, and the relation between h and f as temporal integration. Then the velocity system (16) becomes

$$\frac{v(u_m;s)}{f(s)} = \frac{1}{2\phi}e^{-\tau_{u_m}s}\begin{cases} Q(s), & u_m \geq 0, \\ \overline{Q}(s), & u_m \leq -\varepsilon, \end{cases} \tag{18}$$

where

$$\begin{aligned} Q(s) &= 1+A(s), \quad A(s) = \left(1-e^{-\tau_\varepsilon s}\right)G_{h0}(s), \\ \overline{Q}(s) &= 1+\overline{A}(s), \quad \overline{A}(s) = (1-e^{\tau_\varepsilon s})\,G_{h0}(s). \end{aligned} \tag{19}$$

As the distance between actuators, ε, becomes smaller, we obtain the limits

$$\begin{aligned} \lim_{\varepsilon\to 0}A(s) &= \frac{s}{s+\eta}, \quad \lim_{\varepsilon\to 0}\overline{A}(s) = \frac{-s}{s+\eta}, \\ \lim_{\varepsilon\to 0}Q(s) &= \frac{2s+\eta}{s+\eta}, \quad \lim_{\varepsilon\to 0}\overline{Q}(s) = \frac{\eta}{s+\eta}, \end{aligned}$$

whereas as the free parameter, η, becomes smaller, the limits become

$$\begin{aligned} \lim_{\eta\to 0}A(s) &= 1, \quad \lim_{\eta\to 0}\overline{A}(s) = -1, \\ \lim_{\eta\to 0}Q(s) &= 2, \quad \lim_{\eta\to 0}\overline{Q}(s) = 0. \end{aligned} \tag{20}$$

The limits of $A(s)$ and $\overline{A}(s)$ in (20) indicate that a simultaneous temporal integration and spatial differentiation, as imposed by the rule (17), dictates how the control input is shaped, as two waves equal in absolute amplitude but flipped in sign, with one wave traveling in the positive u direction and the second wave in the negative. Since an actuation by $f(t)$ alone generates two waves equal both in absolute amplitude and in sign, its coordinated operation with $h(t)$ cancels out one of the waves while doubling the other and thus creating a uni-directional wave. This result is expressed by the limits of $Q(s)$ and $\overline{Q}(s)$ in

(20), representing the wave $v(u_m,t)=\frac{1}{\phi}f(t-\tau_{u_m})U(t-\tau_{u_m})$ in (18), which travels in the positive u direction only. This wave is a pure shift of the input $f(t)$ due to pure delay system dynamics in the undamped case.

In practice, however, the physical distance ε between two concentrated actuators cannot be rendered exactly zero. The design parameter η cannot be set exactly to zero either since it will contribute a pole at the origin to the open loop system, i.e. will lead to unbounded h signal for bounded persistent signals f. The wave generated in the positive direction will therefore always remain *near* uni-directional, with amplitude determined by $Q(s)$, and there will always be a residual back-wave with amplitude determined by $\overline{Q}(s)$. The back wave amplitude can be traded-off between the available control effort (f and h grow as ε and η become smaller) and the performance, as discussed in the simulation section, Sec. IV-C. In the actual damped case $\beta>0$, the relation between inputs f and h, (17), evolves to

$$h(s)=G_h(s)f(s),\qquad G_h(s)=\frac{1}{\tau_\varepsilon\left(\lambda(s)+\eta\right)}. \tag{21}$$

The response (18) becomes

$$\frac{v(u_m;s)}{f(s)}=\frac{s}{2\phi\lambda(s)}e^{-\tau_{u_m}\lambda(s)}\begin{cases}Q_\beta(s), & u_m\geq 0,\\ \overline{Q}_\beta(s), & u_m\leq-\varepsilon,\end{cases} \tag{22}$$

where

$$\begin{aligned}&Q_\beta(s)=1+A_\beta(s),\quad A_\beta(s)=\left(1-e^{-\tau_\varepsilon\lambda(s)}\right)G_h(s),\\ &\overline{Q}_\beta(s)=1+\overline{A}_\beta(s),\quad \overline{A}_\beta(s)=\left(1-e^{\tau_\varepsilon\lambda(s)}\right)G_h(s).\end{aligned} \tag{23}$$

We note that the limits (20) remain unchanged, preserving the near uni-directional effect. The wave shape, however, evolves during motion according to the fractional order system dynamics of the damped system.

B. Control of a Single Ring Element

The main focus of this paper is the control of waves in a ring, whose model is given by (6) with the underlying TF described by (7) - (10). As was described in Sec. III-A, this control is accomplished using a combination of two inputs $h(t)$ and $f(t)$, that generate a near uni-directional wave as in (22), which can be used to suppress the waves stemming from (6). To accommodate both the regressive and progressive components of the response in (6), we propose that the control input consist of two pairs, $\{f_1,h_1\}$ and $\{f_2,h_2\}$, located at $\{u_1,u_1+\varepsilon\}$ and $\{u_2,u_2-\varepsilon\}$, respectively (see Fig. 5). Defining $\tau_{u_1}=\frac{u_1}{c}$ and $\tau_{u_2}=\frac{u_2}{c}$, the total open loop response to Ψ is then given by

$$\begin{aligned}&v(u;s)=\\ &\Big[\left(Q_\beta(s)e^{-(\tau-\tau_u+\tau_{u_1})\lambda(s)}+\overline{Q}_\beta(s)e^{-(\tau_u-\tau_{u_1})\lambda(s)}\right)f_1(s)\\ &+\left(Q_\beta(s)e^{-(\tau-\tau_u+\tau_{u_2})\lambda(s)}+\overline{Q}_\beta(s)e^{-(\tau_{u_2}-\tau_u)\lambda(s)}\right)f_2(s)\\ &+\left(e^{-(\tau_u-\tau_{u_0})\lambda(s)}+e^{-(\tau-\tau_u+\tau_{u_0})\lambda(s)}\right)\Psi(s)\Big]\frac{s}{2\phi\lambda(s)\Delta(s)},\end{aligned} \tag{24}$$

which was arbitrarily calculated at $u_1<u<u_2$. At other locations along the ring the times that take the waves generated by f_1 and f_2 reach the point u (here $\tau_u-\tau_{u_j}$ and $\tau-\tau_u+\tau_{u_j}$, $j=1,2$) are changed accordingly. The expression in (24) comprises a response to a disturbance $\Psi(s)$ and to augmented control inputs f_1 and f_2. The latter consist of forward waves and back-waves, whose amplitudes are respectively defined by $Q_\beta(s)$ and $\overline{Q}_\beta(s)$.

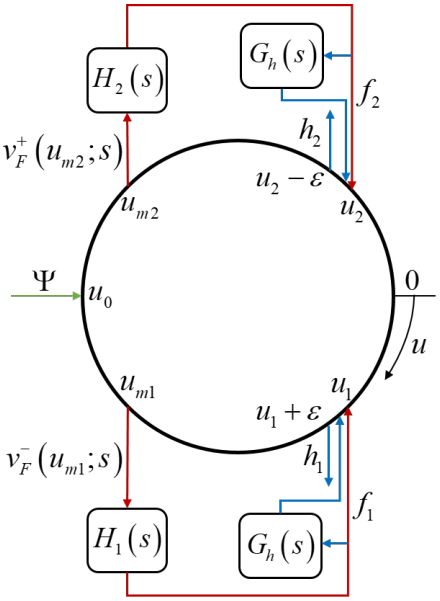

Fig. 5. Control setup for a single ring element. The near uni-directional wave mechanism is generated by the pairs of control signals $\{f_1,h_1\}$ (regressive wave - counterclockwise) and $\{f_2,h_2\}$ (progressive wave - clockwise). $H_1(s)$, $H_2(s)$ and $G_h(s)$ are the controllers designed in (31) and (21). $v_F^-(u_{m_1};s)$ and $v_F^+(u_{m_2};s)$ are the regressive and progressive waves measured at u_{m_1} and u_{m_2}, respectively, and decoupled according to (28). The only requirement for the control locations is $u_2>u_{m_2}>u_{m_1}>u_1$. $\Psi(t)$ is an external disturbance penetrating the ring at u_0, which may be anywhere along the ring.

C. Controller design

The measurements, carried out at u_{m_1} and u_{m_2}, correspond to the regressive and progressive wave components of v, denoted by $v^-(u_{m_1};s)$ and $v^+(u_{m_2};s)$ at these locations, where $v(u_{m_j};s)=v^-(u_{m_j};s)+v^+(u_{m_j};s)$. In a power system example, such a uni-directional measurement may be possible by measuring both swing frequency and power flow at $u=u_{m_j}$, since power flow is defined by the spatial derivative of the swing angle. Another option is measuring at two close points and applying an algorithm similar to that in Sec. III-A to isolate the uni-directional component. Noting that the system response is given by (24), what remains to be determined is the choice of $f_1(s)$ and $f_2(s)$,

$$f_1(s)=-H_1(s)v^-(u_{m_1};s),\quad f_2(s)=-H_2(s)v^+(u_{m_2};s), \tag{25}$$

with controllers $H_1(s)$ and $H_2(s)$ to be properly designed. At each location $\{u_j,u_j\pm\varepsilon\}$, $j=1,2$, a uni-directional control wave is generated by f_j and h_j as described in Sec. III-A. At $\{u_1,u_1+\varepsilon\}$ it is a wave traveling counterclockwise and designed, through $H_1(s)$, to suppresses the regressive disturbance wave, whereas at $\{u_2,u_2-\varepsilon\}$ it is a wave traveling clockwise and designed, through $H_2(s)$, to suppresses the progressive

disturbance wave. In order to design the requisite closed-loops, we take a closer look at the measurements. Arbitrarily assuming that Ψ acts at $u_{m_1} \le u_0 \le u_{m_2}$, the measurements are given by

$$\begin{aligned} v^-(u_{m_1};s) &= \Big[e^{-\left(\tau-\tau_{m_1}+\tau_{u_1}\right)\lambda(s)}Q_\beta(s)f_1(s) \\ &\quad +e^{-\left(\tau_{u_2}-\tau_{m_1}\right)\lambda(s)}\overline{Q}_\beta(s)f_2(s) \\ &\quad +e^{-\left(\tau_{u_0}-\tau_{m_1}\right)\lambda(s)}\Psi(s)\Big]\frac{s}{2\phi\lambda(s)\Delta(s)}, \\ v^+(u_{m_2};s) &= \Big[e^{-\left(\tau-\tau_{u_2}+\tau_{m_2}\right)\lambda(s)}Q_\beta(s)f_2(s) \\ &\quad +e^{-\left(\tau_{m_2}-\tau_{u_1}\right)\lambda(s)}\overline{Q}_\beta(s)f_1(s) \\ &\quad +e^{-\left(\tau_{m_2}-\tau_{u_0}\right)\lambda(s)}\Psi(s)\Big]\frac{s}{2\phi\lambda(s)\Delta(s)}, \end{aligned} \tag{26}$$

where $\tau_{m_1}=\frac{u_{m_1}}{c}$ and $\tau_{m_2}=\frac{u_{m_2}}{c}$. For Ψ acting at a different location, its arrival times to u_{m1} and u_{m_2}, given by $\tau_{u_0}-\tau_{m_1}$ and $\tau_{m_2}-\tau_{u_0}$, will accordingly change. Since a measurement at u_{m_1} (u_{m_2}) contains the back-wave of the measurement at u_{m_2} (u_{m_1}) through $\overline{Q}_\beta(s)$, the $H_1(s)$ loop is coupled with the $H_2(s)$ loop. To eliminate the coupling from the feedback, we calculate and subtract the back-waves from the measurements, replacing (25) with

$$f_1(s)=-H_1(s)v_F^-(u_{m1};s), \quad f_2(s)=-H_2(s)v_F^+(u_{m2};s), \tag{27}$$

where $v_F^-(u_{m1};s)$ and $v_F^+(u_{m2};s)$ are 'filtered' measurements given by

$$\begin{aligned} v_F^-(u_{m_1};s) &= \Big[e^{-\left(\tau-\tau_{m_1}+\tau_{u_1}\right)\lambda(s)}Q_\beta(s)f_1(s) \\ &\quad +e^{-\left(\tau_{u_0}-\tau_{m_1}\right)\lambda(s)}\Psi(s)\Big]\frac{s}{2\phi\lambda(s)\Delta(s)}, \\ v_F^+(u_{m_2};s) &= \Big[e^{-\left(\tau-\tau_{u_2}+\tau_{m_2}\right)\lambda(s)}Q_\beta(s)f_2(s) \\ &\quad +e^{-\left(\tau_{m_2}-\tau_{u_0}\right)\lambda(s)}\Psi(s)\Big]\frac{s}{2\phi\lambda(s)\Delta(s)}. \end{aligned} \tag{28}$$

Such decoupling is assumed to be achievable since the subtracted expressions are the control inputs, which are known in real time. The decoupled measurements (28) lead to the control inputs

$$f_j(s)=-\frac{H_j(s)\frac{s}{2\phi\lambda(s)}e^{-|\tau_{u_0}-\tau_{m_j}|\lambda(s)}}{\Delta_{CL}(s)}\Psi(s), \quad j=1,2 \tag{29}$$

where $\Delta_{CL}(s)$ is the closed loop counterpart of $\Delta(s)$, given by

$$\Delta_{CL}(s)=\Delta(s)+H_j(s)\frac{s}{2\phi\lambda(s)}Q_\beta(s)e^{-\left(\tau-|\tau_{u_0}-\tau_{m_j}|\right)\lambda(s)}. \tag{30}$$

To achieve elimination of the circulation exponent $e^{-\tau\lambda(s)}$ from $\Delta_{CL}(s)$, we set the controllers $H_j(s)$ in (27) to

$$H_j(s)=\frac{2\phi\lambda(s)}{s}\frac{1}{Q_\beta(s)}e^{-|\tau_{m_j}-\tau_{u_j}|\lambda(s)}, \quad j=1,2 \tag{31}$$

which is acceptable due to stability of $\frac{s}{\lambda(s)\Delta(s)}$ and $Q_\beta(s)$. The expression of $H_j(s)$ in (31) and the elimination of the circulation exponent out of $\Delta_{CL}(s)$ is independent of the disturbance origin u_0. The closed loop response then becomes a sum of forward and backward waves,

$$v(u;s)=v_{\text{forward}}(u;s)+v_{\text{back}}(u;s), \tag{32}$$

where

$$\begin{aligned} v_{\text{forward}}(u;s) &= \frac{s}{2\phi\lambda(s)}e^{-\left(\tau_u-\tau_{u_0}\right)\lambda(s)}\Psi(s) \\ v_{\text{back}}(u;s) &= -\frac{s}{2\phi\lambda(s)\Delta(s)}\frac{\overline{Q}_\beta(s)}{Q_\beta(s)}\left[e^{-\theta_{B1}\lambda(s)}+e^{-\theta_{B2}\lambda(s)}\right]\Psi(s), \end{aligned} \tag{33}$$

and for u and u_0 at $[u_{m_1},u_{m2}]$, we have

$$\theta_{B1}=\tau-\tau_u+2\tau_2-\tau_{u_0}, \quad \theta_{B2}=\tau_u+\tau_{u_0}-2\tau_1. \tag{34}$$

For different locations of u and disturbance origin u_0, the arrival times θ_{B1} and θ_{B2} are changed accordingly. Result (32)-(34) states that the IWS control method, given by (21), (27) and (31), completely absorbs propagating waves at the artificial active boundaries at u_1 and u_2 (no $\Delta(s)$ in the forward waves in (33)). This means that the forward waves cannot 'escape' from the region $u_1<u<u_2$. The closed loop response (33) is thus confined only to the unavoidable back-waves that are decoupled in (28) and are unaffected by the control algorithm. This closed loop system is stable, as proved in detail in Sec. V. We summarize the proposed control strategy and the resulting closed loop system performance in the following theorem.

Theorem 3.1: We consider the continuous system in (15), where $y(t)$ is the response to control inputs $f(t)$ and $h(t)$ (see Fig. 4). A controller using the Interior Wave Suppression algorithm described by (21), (27) and (31) is guaranteed to achieve complete suppression of any wave circulation produced by disturbances. The resulting closed loop system is stable.

Proof. The proof of the control mechanism is obvious from Section III-C. The closed loop system stability is proved in Sec. V. □

We conclude this section with a note on a more realistic case of finite actuation bandwidth, where the control input TF (22) contains also some actuator dynamics, e.g. defined by $\frac{1}{\mu_f s+1}$. The controllers (31) can then increase the possibly too slow closed loop dynamics by introducing a faster one, i.e. contain also a lead term $\frac{\mu_f s+1}{\mu_H s+1}$, where $\mu_H<\mu_f$. The closed loop response will then include also a portion of the forward waves whose characteristic equation is given by

$$\Delta_\mu(s)=1-\frac{\mu_H s}{\mu_H s+1}e^{-\tau\lambda(s)}, \tag{35}$$

which approaches 1 as μ_H tends to zero, retrieving the ideal case (33), and which is stable for any $\beta>0$ (Sec. V).

D. Modeling and control of a network of rings

Control, observation, and stabilization of PDE's, and in particular, wave equations on networks is a subject of a large amount of literature, [37], [38], [39], [40], to name a few. In most of the reports the considered network topology is a collection of strings with open ends, i.e. tree or star connections, where the control is performed at the nodes. The availability of the open ends enables to utilize the control at the exterior nodes for system stabilization, similar to the boundary control setups. In our case, though, no open ends are

assumed and the control is performed at the ring interior. We therefore would like to study the extension of the single ring IWS control algorithm to a network of several rings connected together at a point or along a line.

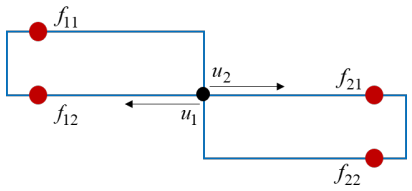

Fig. 6. A diagram of a two-ring network connected at a single node (black spot). f_{j1} and f_{j2} (red spots), $j=1,2$, indicate uni-directional wave generators. u_1 and u_2 are the spatial coordinates of the left and right rings, respectively.

The first step to do so is derivation of an appropriate TF model. Although there is no general formula for an arbitrarily connected system of rings, the model can be constructed by applying the two basic connectivity laws of continuity of 'position' (swing angle) and balance of 'forces' (electrical power flow) at each node.

For example, consider the top-left and the bottom rings of the network depicted in Fig. 1-(b), connected at a single point and given again schematically in Fig. 6. Each ring is governed by the wave equation (1) with corresponding position variables y_1 and y_2, representing left and right rings, respectively, and with respective spatial coordinates u_1 and u_2, both originating at the node. Let the left and right rings have the properties $\{T_1,\rho_1,L_1\}$ and $\{T_2,\rho_2,L_2\}$, leading to $\{\phi_1,c_1\}$ and $\{\phi_2,c_2\}$. At the node, the position continuity condition is given by

$$y_1(u_1=0,t)=y_2(u_2=0,t)=y_1(u_1=L_1,t)=y_2(u_2=L_2,t),$$

whereas the balance of forces, assuming for brevity a disturbance $\Psi(t)$ at the node, reads

$$\begin{aligned}\Psi(t)+T_1\left[y_{1\_u_1u_1}(u_1=L_1,t)-y_{1\_u_1u_1}(u_1=0,t)\right]\\ =T_2\left[y_{2\_u_2u_2}(u_2=0,t)-y_{2\_u_2u_2}(u_2=L_2,t)\right].\end{aligned}$$

The resulting TFs from $\Psi(t)$ to the velocity (swing frequency) of each ring, for an undamped system become

$$\begin{aligned}\frac{v_1(u_1;s)}{\Psi(s)}&=\frac{1}{\Delta_{12}(s)}\left(e^{-(\tau_1-\tau_{u_1})}s+e^{-\tau_{u_1}s}\right)\left(1+e^{-\tau_2 s}\right)\\ \frac{v_2(u_2;s)}{\Psi(s)}&=\frac{1}{\Delta_{12}(s)}\left(e^{-(\tau_2-\tau_{u_2})}s+e^{-\tau_{u_2}s}\right)\left(1+e^{-\tau_1 s}\right)\end{aligned}$$

where $\tau_1=\frac{L_1}{c_1}$, $\tau_2=\frac{L_2}{c_2}$, $\tau_{u_1}=\frac{u_1}{c_1}$ and $\tau_{u_2}=\frac{u_2}{c_2}$, and the characteristic equation is given by

$$\Delta_{12}(s)=\left(1-e^{-\tau_1 s}\right)\left(1+e^{-\tau_2 s}\right)\phi_1+\left(1+e^{-\tau_1 s}\right)\left(1-e^{-\tau_2 s}\right)\phi_2.$$

The physical implication of these TFs is that a wave approaching the node along one path is split to four components: three of them are waves proceeding to the remaining three paths, and the forth is a reflected wave that in total yields 1.

Similarly to the extension of the model from a single ring to a network of rings, the corresponding control design might be extended as well. A possible option would be to place a pair of uni-directional wave generators f_1,h_1 and f_2,h_2 at each link between two nodes, which obey the strategies in (21), (25) and (31), and denoted by the red circles in Fig. 6. At each ring f_1,h_1 will suppress the progressive waves, and f_2,h_2 the regressive. The complexity, however, arises in the process of the measurement decoupling, which was described in (28) for the single-ring case. Since the network in Fig. 6 includes four control waves, there are four back-waves and also reflections of the forward waves. The decoupling process of each uni-directional measurement should therefore be adjusted accordingly.

IV. Implementation of the IWS control in an actual grid and simulations

In this section we consider the practical aspects of the IWS control methodology, designed in the previous section. Specifically, we first discuss the implementation of the controllers proposed in (21), (25) and (31) due their fractional order. We then suggest how to incorporate these controllers and the required measurements in an actual power system.

A. Implementation of the fractional order controllers

The controllers $H_j(s)$ in (31) are of fractional order. Their implementation thus requires rational approximations, for which there exist several methods, both via time and frequency domains. In time domain methods, the impulse response of a suggested finite dimension controller is fitted to the impulse response of the exact controller (if known) by optimization algorithms, see e.g. [20]. The frequency domain methods are based on an analogous optimized fitting of the frequency response, such as [41], for systems with infinite number of singularities. Several methods were also reported in [42], [43] and [44]. Since $H_j(s)$ are relatively simple with only two branch point singularities, standard software algorithms are sufficient, where the frequency response is calculated on the principal surface. However, if the phase of a fractional order function begins or ends at non-integer multiples of 90°, the approximation usually has large errors. For example, the phase of the $\frac{\lambda(s)}{s}$ component at $s=j\omega$ (in the expression of $H_j(s)$) equals 45° at $\omega=0$. For that reason, we do not approximate $\frac{\lambda(s)}{s}$ directly, but first rewrite it as $\frac{\lambda(s)}{s}=\frac{R(s)-\frac{1}{2}\beta}{s}+\frac{\frac{1}{2}\beta}{s}+1$, where $R(s)=\lambda(s)-s$. Since the phase of the strictly proper $R(s)-\frac{1}{2}\beta$ ranges from 180° to 90°, we apply the fitting algorithm directly to it. The approximation of other fractional order expressions is carried out in a similar way. Figure 7 depicts the actual fitting of the frequency responses and the resulting fitting of the impulse responses of the exact $\frac{\lambda(s)}{s}$ and its approximation by a third order rational controller.

B. Implementation in an actual generators chain

The Interior Wave Suppression control approach for a ring can be summarized as follows: choose two pairs of control inputs, f_1,h_1 located at u_1 and $u_1+\varepsilon$, and f_2,h_2, located at u_2 and $u_2-\varepsilon$, two velocity measurements, regressive at u_{m_1} and progressive at u_{m_2}, and apply control strategies specified by (21), (25), (28) and (31). The question that we address in this section is the actual actuation quantities in a power system that the f_j and h_j inputs will correspond to. As was

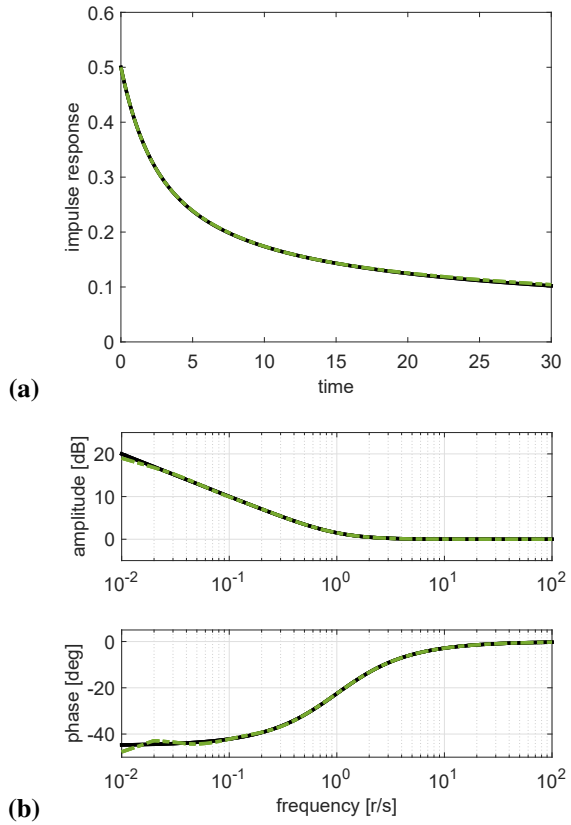

Fig. 7. **(a)**: impulse response of $\frac{\lambda(s)}{s}-1$, the strictly proper part of the $\frac{\lambda(s)}{s}$ component of $H(s)$. **(b)**: frequency response of the $\frac{\lambda(s)}{s}$ component of $H(s)$. Solid-black: exact, dashed dotted-green: 3-rd order rational approximation.

discussed in Sec. I, the commonly used actuation methods in power grid control are mechanical power injection and tie-line reactance variation, respectively denoted by the deviation variables $\widetilde{P}^M(t)=P^M(t)-\overline{P}^M$ and $\widetilde{X}(t)=X(t)-\overline{X}$, where the overhead bar denotes the equilibrium state.

Returning to the discrete model (2) and linearizing around an equilibrium power flow $\overline{P}^E$, the effect of the linearized control inputs $\widetilde{P}^M(t)$ and $\widetilde{X}(t)$ can be shown to result in

$$\begin{aligned}\tfrac{2HS}{\Omega}\ddot{y}_j &= \tfrac{1}{\overline{X}}\left[y_{j+1}-2y_j+y_{j-1}\right]+\tfrac{\overline{P}^E}{\overline{X}}\widetilde{X}+\widetilde{P}^M,\\ \tfrac{2HS}{\Omega}\ddot{y}_{j+1} &= \tfrac{1}{\overline{X}}\left[y_{j+2}-2y_{j+1}+y_j\right]-\tfrac{\overline{P}^E}{\overline{X}}\widetilde{X},\end{aligned} \tag{36}$$

for generators $j-1$, j and $j+1$ adjacently spaced in a ring of N generators. At the spatially continuous limit and transformed to Laplace domain, (36) becomes

$$\begin{aligned}\left(\tfrac{s}{c}\right)^2 y(u;s) = y_{uu}(u;s)+\tfrac{1}{T}\left[\widetilde{P}^M(s)+T\overline{P}^E\widetilde{X}(s)\right]\widehat{\delta}(u-u_0)\\ -\tfrac{1}{T}\left[T\overline{P}^E\widetilde{X}(s)\right]\widehat{\delta}(u-(u_0-\varepsilon)),\end{aligned} \tag{37}$$

where $T=\frac{\varepsilon}{\overline{X}}$, $c=\sqrt{\frac{\Omega\varepsilon^2}{2HS\overline{X}}}$ and ε is the distance between adjacent generators. As (37) has the same form as (4), it follows that $\widetilde{P}^M$ corresponds to the f input and $\frac{1}{\varepsilon x}\overline{P}^E\widetilde{X}$ to the h input. A physical reasoning is that $\widetilde{P}^M$ directly affects only the particular generator to which it is injected, whereas the reactance variation $\widetilde{X}$ inversely affects the adjacent generators it operates in between.

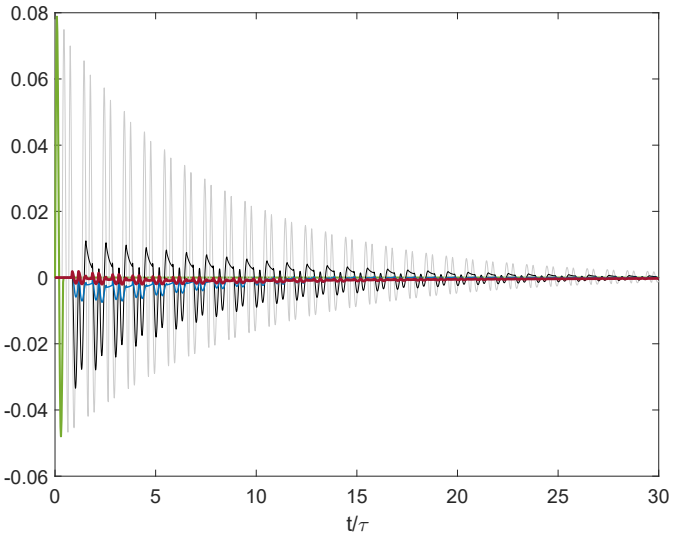

Fig. 8. $v(u,t)$ at $u=0.85L$ in response to $\Psi(t)$ (green, 0.5 scaled) in Example 4.1. Open loop (gray) versus closed loop for different values of η in (21): $\eta=\frac{1}{5}\tau$ (red), $\eta=\tau$ (blue) and $\eta=5\tau$ (black).

C. Simulations

Example 4.1: We consider again the power grid system in Example 2.1 with the realistic numerical values therein, describing a ring of 200 generators evenly spanned across 6400_{km}, yielding distance between generators of $\varepsilon=32_{km}$. This time the system is controlled in closed loop with the Interior Wave Suppression controllers given by (21), (25) and (31). The damping constant was assumed $\beta=0.1$ in appropriate units. The same vanishing pulse disturbance $\Psi(t)=0.1S\sin\frac{5\pi t}{\tau}\left[U(t)-U(t-0.4\tau)\right]$ penetrates the ring at $u_0=\frac{1}{2}L$. The actuation and measurement locations were respectively set to $u_1=0.25L$ and $u_2=0.75L$, and $u_{m1}=0.35L$ and $u_{m2}=0.65L$. The actuator dynamics constant is set to $\mu_f=0.01$, whereas the controller lead compensator constant is $\mu_H=\mu_f/100$.

Figure 8 depicts the response at $u=0.85L$ to the concentrated input $\Psi(t)$ (green, 0.5 scaled). The open loop response (gray) is plotted versus the closed loop response for several values of the design parameter η in (21), including $\eta=\frac{1}{5}\tau$ (red), $\eta=\tau$ (blue) and $\eta=5\tau$ (black), where $\tau\approx 2.5_s$. The smaller is η, the closer to zero is the limit of the back wave amplitude (20), leading to a smaller back wave. Figure 9 depicts the actual power grid control inputs $\widetilde{X}_1$ (a) and $\widetilde{P}_1^M$ (b) (respectively identical to $\widetilde{X}_2$ and $\widetilde{P}_2^M$ due to symmetry). The plot exhibits the trade-off of wave suppression with the energy of control inputs $\widetilde{X}_j$, whose convergence is slower and amplitude is higher for smaller η. $\widetilde{P}_j^M$ are independent of η.

V. Stability Analysis of the Single-Ring Case

The closed-loop control setup for a continuous single-ring model consists of two pairs of actuators, $\{f_1,h_1\}$ and $\{f_2,h_2\}$, and two respective measurements, $v^-(u_{m_1};s)$ and $v^+(u_{m_2};s)$,

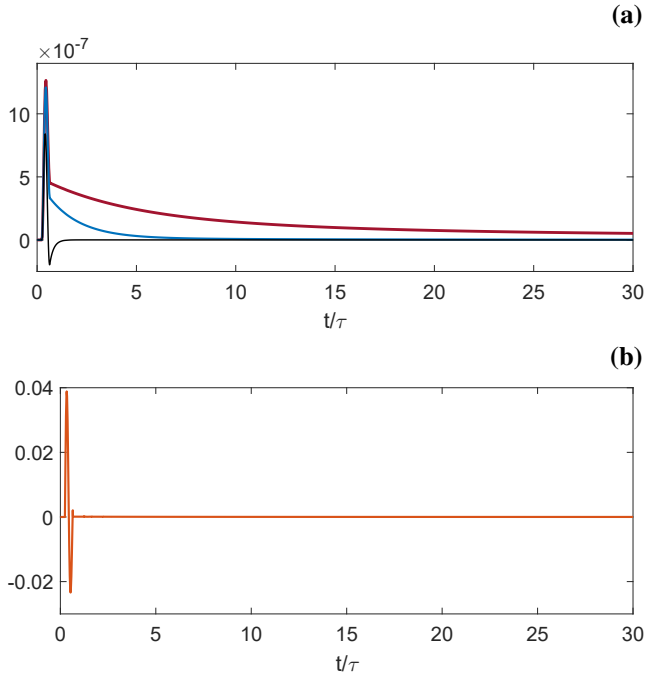

Fig. 9. Control signals in closed loop of Example 4.1. **(a)** , $\widetilde{X}_1$ for $\eta = \frac{1}{5}\tau$ (red), $\eta = \tau$ (blue) and $\eta = 5\tau$ (black). **(b)** $\widetilde{P}_1^M$ (orange, independent of η).

as illustrated in Fig. 5. The controllers $H_1(s)$ and $H_2(s)$ correspond to the Interior Wave Suppression strategy, specified by (21), (25) and (31). The closed loop TF between an external disturbance $\Psi(t)$ and the velocity response was derived in (33). The complete transfer matrix between all possible signals in the closed loop, including unmodeled signals such as actuation uncertainties and measurement noise, is given by

$$\begin{bmatrix} \mathbf{y} \\ \mathbf{f} \end{bmatrix} = \begin{pmatrix} \mathbf{G_{yd}} & \mathbf{G_{yn}} \\ \mathbf{G_{fd}} & \mathbf{G_{fn}} \end{pmatrix} \begin{bmatrix} d \\ \mathbf{n} \end{bmatrix}. \tag{38}$$

Here $\mathbf{y}$ is the outputs vector including the swing frequency at any point u and at the measurement points u_{mj}. $\mathbf{f}$ is the controls vector including the h_j signals (f_j are not included since their stability is guaranteed by that of h_j). d is a representative disturbance signal that stands for the power disturbance ψ and actuation disturbances d_{f_1}, d_{f_2}, d_{h_1}, d_{h_2}, all entering the loop through the same TF (7) with a difference only within the exponent arguments, indicating the relative locations of the disturbance action and the output. $\mathbf{n}$ is the measurement noises vector. All these signals are given by

$$\mathbf{y} = \begin{bmatrix} v(u;s) & v_F^-(u_{m1};s) & v_F^+(u_{m2};s) \end{bmatrix}' \tag{39a}$$
$$\mathbf{f} = \begin{bmatrix} h_1(s) & h_2(s) \end{bmatrix}' \tag{39b}$$
$$d = \psi(s) \tag{39c}$$
$$\mathbf{n} = \begin{bmatrix} n_{v1}(s) & n_{v2}(s) \end{bmatrix}'. \tag{39d}$$

The sub-matrices in (38) are given by

$$\begin{aligned}
\mathbf{G_{yd}}(s) &= \frac{G_1(s)}{2\phi\Delta_\mu(s)} \begin{bmatrix} \left[G_{\theta_1}(s)+G_{\theta_2}(s)\right] - B(s) \\ G_{\theta_5}(s) \\ G_{\theta_6}(s) \end{bmatrix}, \\
\mathbf{G_{fd}}(s) &= \frac{G_h(s)}{Q_\beta(s)} \begin{bmatrix} G_{\theta_7}(s) \\ G_{\theta_8}(s) \end{bmatrix}, \\
\mathbf{G_{yn}}(s) &= -\begin{bmatrix} G_{\theta_9}(s)+G_{\theta_{10}}(s) \\ G_{\theta_\tau}(s) \\ G_{\theta_\tau}(s) \end{bmatrix}, \\
\mathbf{G_{fn}}(s) &= \frac{2\phi G_0^{-1}(s)}{Q_\beta(s)} \begin{bmatrix} G_{\theta_{11}}(s) \\ G_{\theta_{12}}(s) \end{bmatrix},
\end{aligned} \tag{40}$$

where

$$\begin{aligned}
B(s) &= Q_\beta^{-1}(s) G_0(s) \overline{Q}_\beta(s) \left[G_{\theta_3}(s)+G_{\theta_4}(s)\right], \\
G_1(s) &= \frac{s}{\lambda(s)}, \quad G_0(s) = \frac{G_1(s)}{\Delta(s)}, \quad G_\theta(s) = e^{-\theta\lambda(s)}.
\end{aligned} \tag{41}$$

$Q_\beta(s)$ and $\overline{Q}_\beta(s)$ are defined in (23) and $G_h(s)$ in (21), $\Delta_\mu(s)$ in (35), and $\Delta(s)$, $\lambda(s)$ and ϕ in (8), (5) and (10). θ in $G_\theta(s)$ stands for any of the exponent arguments $\theta_\tau = \tau$ and $\theta_1 \div \theta_{12}$, whose exact expressions are given by

$$\begin{aligned}
\theta_1 &= \tau_u - \tau_\psi & \theta_2 &= \tau - \tau_u + \tau_\psi \\
\theta_3 &= \tau + \tau_u - 2\tau_1 + \tau_\psi & \theta_4 &= 2\tau_2 - \tau_u - \tau_\psi \\
\theta_5 &= \tau - \tau_{m_1} + \tau_\psi & \theta_6 &= \tau_{m_2} - \tau_\psi \\
\theta_7 &= \tau - \tau_{u_1} + \tau_\psi & \theta_8 &= \tau_{u_2} - \tau_\psi \\
\theta_9 &= \tau - \tau_u + \tau_{m_1} & \theta_{10} &= \tau - \tau_{m_2} + \tau_u \\
\theta_{11} &= \tau_{m_1} - \tau_{u_1} & \theta_{12} &= \tau_{u_2} - \tau_{m_2}.
\end{aligned} \tag{42}$$

In this section, we show that the complete closed-loop system (38)-(42) is stable invoking the internal stability criterion, which claims that the closed loop system is stable provided that TFs from all possible inputs to all possible outputs are stable. These, in turn, are captured by the transfer matrix in (38), which consists of finite summations or multiplications of the systems $G_\theta(s)$, $G_0(s)$, $G_1(s)$, $G_0^{-1}(s)$, $G_h(s)$, $Q_\beta(s)$, $Q_\beta^{-1}(s)$, $\overline{Q}_\beta(s)G_\theta(s)$ and $\Delta_\mu(s)$. The goal of this section is therefore proving stability of each of the above listed TFs.

Since $\beta > 0$, the underlying TFs are all of fractional order. Stability of fractional order systems is a non-trivial problem that has received increased attention in recent years. Since these systems are irrational, their stability analysis cannot, in general, be limited to pole location only, as was discussed in [45] for fractional order characteristic polynomials of s^γ, $\gamma \in (0,1)$. In a series of recent publications [46], [47], [48], stability of such polynomials, with the addition of integer order time delays, were investigated. The situation here is quite different because the model (7) includes fractional order delays, specifically exponents of $\lambda(s) = (s^2+\beta s)^{1/2}$, so the results of the above listed publications are not directly applicable.

We choose to carry out the stability analysis of our system mainly in time domain following the L^1 stability criterion, which was defined in [45] as:

Definition 5.1: A TF $G(s)$, defined by its impulse response $\mathscr{G}(t) = \tilde{\mathscr{G}}(t) + \sum g_k \delta(t-t_k)$, is stable in L^1 sense iff:

$$\forall u(t) \in L^\infty, \quad y(t) = \mathscr{G}(t) \star u(t) \in L^\infty, \tag{43}$$

which is satisfied when $\tilde{\mathscr{G}}(t) \in L^1$ and $|g_k| < \infty$. The assumed time domain of all signals is the non-negative real axis.

Although stability in the L^1 sense guarantees stability in the H^∞ sense, for some TFs we add a direct H^∞ stability proof. This advocates the validity of the complex domain stability analysis for the fractional order systems at hand, which for particular TFs we use in a standalone manner.

Proposition 5.2: All the components of the complete closed loop system (38), which are given by $G_\theta(s)$, $G_0(s)$, $G_1(s)$, $G_0^{-1}(s)$, $G_h(s)$, $Q_\beta(s)$, $Q_\beta^{-1}(s)$, $\overline{Q}_\beta(s)G_\theta(s)$ and $\Delta_\mu(s)$ in (41), are stable.

Proof. The proof is given in Appendix A. □

VI. Conclusion

We consider the problem of wave propagation in a ring, which is a common phenomenon in several engineering problems including that of a power grid. Rather than viewing the underlying oscillations using discrete-space models, we propose a continuous approach to model the problem and a model-based control to suppress the waves. A ring topology with a one-dimensional wave equation is used to analyze the underlying dynamics. The Interior Wave Suppression (IWS) method was used as the underlying control method.

The main difficulty introduced due to the ring geometry is the lack of boundaries, and therefore any concentrated input to the ring generates waves in two directions, both progressive and regressive, thereby preventing total absorption. Using a judicious combination of control inputs it is shown that a near uni-directional wave can be generated, with minimal back-waves. Two pairs of coordinated control inputs are used in particular, each operating at a different location along the ring so as to match the circulating progressive and regressive waves. Two independent velocity measurements are used for feedback with suitable filtering introduced so that the effects of the two control back-waves at the measurement location are decoupled from each other. The decoupling process enables the disturbance suppression by the forward control waves, while the residual back-waves, whose amplitudes are reduced by the IWS algorithm, decay according to the open loop damping.

Any damping present in the system was included, leading to fractional order transfer function model and associated IWS controllers, which were accommodated through appropriate analysis. The resulting closed-loop system is proved to be stable. The overall modeling and control methods are shown to be implementable in a power grid using PMU as sensors and FACTS devices such as TCSC as actuators. Numerical simulations demonstrate that the proposed method is viable and leads to satisfactory suppression of waves.

Appendix A
Proof of Proposition 5.2 in Sec. V

Stability of $G_\theta(s)$:

Proof. We invoke the time domain criterion 5.1. $G_\theta(s)$ is proper but not strictly proper. Extracting its delayed component $e^{-\theta\lambda(s)} = e^{-\theta s}e^{-\theta R(s)}$, where $R(s) = \lambda(s) - s$ (as was defined in Sec. IV), and the bound of the causal component $e^{-\theta R(s)}$ at the right half plane (on the principal surface) is given by $e^{-\frac{1}{2}\beta\theta}$. The strictly proper part of $G_\theta(s)$, which we denote by $\widetilde{G}_\theta(s)$, is therefore given by $\widetilde{G}_\theta(s) = G_\theta(s) - e^{-\left(\frac{1}{2}\beta+s\right)\theta}$. Stability of $G_\theta(s)$ will thus immediately stem from the stability of $\widetilde{G}_\theta(s)$, for which we need to calculate the inverse Laplace transform or, equivalently, its impulse response, denoted by $\widetilde{\mathscr{G}}_\theta(t)$. It should be noted that one cannot determine the inverse Laplace transform of $\widetilde{G}_\theta(s)$ easily by using standard tables [31]. We therefore provide its derivation below. The derivative of $\widetilde{G}_\theta(s)$ with respect to s, which we denote by $\widetilde{G}_{\theta\_\mathrm{d}}$, is given by

$$\widetilde{G}_{\theta\mathrm{d}}(s) = \tfrac{\mathrm{d}}{\mathrm{d}s}\widetilde{G}_\theta(s) = -(s+\tfrac{1}{2}\beta)\theta\Gamma(\theta;s) + \theta e^{-\left(\frac{1}{2}\beta+s\right)\theta}, \quad (44)$$

where $\Gamma(\theta;s)$ is defined in (13). Since $\gamma(\theta,t)$ in (14), which is the inverse Laplace transform of $\Gamma(\theta;s)$, is a function delayed by $t=\theta$, we have $s\Gamma(\theta;s) = \mathscr{L}\{\dot{\gamma}(\theta,t)\} + \gamma(\theta,\theta)$, where $\gamma(\theta,\theta) = e^{-\frac{1}{2}\beta\theta}U(t-\theta)$. We therefore obtain

$$\begin{aligned}&\mathscr{L}^{-1}\left\{-s\theta\Gamma(\theta;s) + \theta e^{-\left(\frac{1}{2}\beta+s\right)\theta}\right\} = \dot{\gamma}(\theta,t)\\ &= \tfrac{1}{2}\beta e^{-\frac{1}{2}\beta t}\left(t\frac{I_1\left(\frac{1}{2}\beta\sqrt{t^2-\theta^2}\right)}{\sqrt{t^2-\theta^2}} - I_0\left(\tfrac{1}{2}\beta\sqrt{t^2-\theta^2}\right)\right)U(t-\theta),\end{aligned} \quad (45)$$

where $I_1(\cdot)$ is the 1_{st} order modified Bessel function. Substituting (45) and (13) to (44), the zero order Bessel function is canceled. Applying the Laplace transform integration rule $\mathscr{L}^{-1}\left\{\tilde{G}_\theta(s)\right\} = -\frac{1}{t}\mathscr{L}^{-1}\{\tilde{G}_{\theta\mathrm{d}}(s)\}$, we obtain

$$\widetilde{\mathscr{G}}_\theta(t) = \tfrac{1}{2}\beta\theta e^{-\frac{1}{2}\beta t}\frac{I_1\left(\frac{1}{2}\beta\sqrt{t^2-\theta^2}\right)}{\sqrt{t^2-\theta^2}}U(t-\theta). \quad (46)$$

Now we need to show that $\mathscr{G}_\theta(t)$, the impulse response of $G_\theta(s)$, is absolutely integrable. Since $\widetilde{\mathscr{G}}_\theta(t)$ is continuous and bounded (at $t=\theta$ it equals $\frac{1}{8}\beta^2\theta e^{-\frac{1}{2}\beta\theta}$), it is thus absolutely integrable on a strip $t\in[0,t_1]$ for some finite t_1, so we only need to verify that it is absolutely integrable on $t\in[t_1,\infty)$. For large t, $\sqrt{t^2-\theta^2}\approx t$, and by [32], $\widetilde{\mathscr{G}}_\theta(t)$ has the asymptotic expansion:

$$\widetilde{\mathscr{G}}_\theta(t) \approx \tfrac{1}{2}\beta\theta e^{-\frac{1}{2}\beta t}\frac{I_1\left(\frac{1}{2}\beta t\right)}{t} \sim \frac{C_0}{t\sqrt{t}}\left(1 - \frac{c_1}{t} - \frac{c_2}{t^2} - \frac{c_3}{t^3}\cdots\right), \quad (47)$$

where $C_0 = \frac{\theta}{2}\sqrt{\frac{\beta}{\pi}}$, $c_1 = \frac{3}{4\beta}$, $c_2 = \frac{15}{2!(4\beta)^2}$ and $c_3 = \frac{315}{3!(4\beta)^3}$. Therefore, we obtain

$$\int_{t_1}^{\infty}|\mathscr{G}_\theta(t)|\,\mathrm{d}t \leqslant \int_{t_1}^{\infty}\left|\frac{C_0}{t\sqrt{t}}\right|\mathrm{d}t + \int_{t_1}^{\infty}\left|\frac{C_0c_1}{t^2\sqrt{t}}\right|\mathrm{d}t + \cdots. \quad (48)$$

Since

$$\int_{t_1}^{\infty}\left|t^{-\left(\frac{1}{2}+\varepsilon\right)}\right|\mathrm{d}t < \infty \quad \forall\varepsilon > 0, \quad (49)$$

each integral in (48) converges, yielding $\widetilde{\mathscr{G}}_\theta(t)\in L^1(\mathbb{R}_+)$ and thus $G_\theta(s)$ is stable in the L^1 sense. □

Stability of $G_0(s)$:

Proof. We first prove that $G_1(s)$ is stable and then prove that the division by $\Delta(s)$ does not affect this result. Considering again the L^1 criterion, we isolate the strictly proper component

of $G_1(s)$, which is given by $\widetilde{G}_1(s) = G_1(s) - 1$. The calculation of its inverse Laplace transform, $\mathscr{G}_1(t)$, similarly to G_0, gives

$$\mathscr{G}_1(t) = \tfrac{1}{2}\beta e^{-\frac{1}{2}\beta t}\left(I_1\left(\tfrac{1}{2}\beta t\right) - I_0\left(\tfrac{1}{2}\beta t\right)\right),$$

whose asymptotic expansion, by [32], is given by $\mathscr{G}_1(t) \sim -C_0/\beta(t\sqrt{t})^{-1}\left(c_1 t^{-1} + c_2 t^{-2} + c_3 t^{-3}\cdots\right)$, and is therefore absolutely integrable by the same reasoning of $\mathscr{G}_\theta(t)$.

For a direct proof that $G_1(s)$ is also H^∞ stable we rewrite it as $G_1(s) = \frac{s^{1/2}}{(s+\beta)^{1/2}}$. The singularities (here of branch point type) are located at $s = 0$ and $s = -\beta$, i.e. outside of the open right half plane. It is easy to see that $|G_1(s)| < 1$, which completes the proof for $G_1(s)$.

Proceeding with the complex domain considerations, we now prove that $\Delta(s)$ in the denominator of $G_0(s)$ keeps it analytic and bounded in the open right half plane. Calculating the roots of $\Delta(s) = 0$, we obtain $-\tau\lambda(p) = ln(1) = 2n\pi i$, with $n = 0, \pm 1, \pm 2, \ldots$, whose solutions are given by $p = 0, -\beta, -\frac{1}{2}\beta \pm \sqrt{\left(\frac{1}{2}\beta\right)^2 - \left(\frac{2n\pi}{\tau}\right)^2}$. All roots except for $p = 0$ are located in the open left half plane, spaced symmetrically with respect to the vertical line $-\frac{1}{2}\beta$. The only seemed cause for $G_0(s)$ not to be bounded in the open right half plane is the root $p = 0$ of $\Delta(s)$. However, the effect of this root is annihilated by $G_1(s)$, which renders the total limit of $G_0(s)$ at $s = 0$ to be $\frac{1}{\tau\beta}$, which therefore means $G_0(s)$ is stable. □

Stability of $G_0^{-1}(s) = \frac{\lambda(s)\Delta(s)}{s}$:

Proof. We observe that $G_0^{-1}(s)$ is analytic in the open right half plane. To be bounded as well, $s = 0$ must not be its singularity. However, in the proof of stability of $G_0(s)$ earlier in this section we obtained the limit for $\lim_{s\to 0} G_0(s) = \frac{1}{\tau\beta}$, hence $\lim_{s\to 0} G_0^{-1}(s) = \tau\beta$, which is obviously finite. □

Stability of $G_h(s)$:

Proof. Using complex domain considerations, we need to show that the roots of $\left(s^2 + \beta s\right)^{1/2} + \eta = 0$, the denominator of $G_h(s)$, are all located in the open left half plane. We need to regard only one solution of two that converges to $s = -\eta$ as $\beta \to 0$, and thus obtain $s = -\frac{1}{2}\beta - \frac{1}{2}\left(\beta^2 + 4\eta^2\right)^{1/2}$, which is strictly negative. □

Stability of $Q_\beta(s)$:

Proof. First we write explicitly $Q_\beta(s) = 1 + A_\beta(s) = 1 + G_h(s) - G_h(s)G_\Theta(s)$, where $\Theta = \theta + \tau_\varepsilon$. Stability of $Q_\beta(s)$ is therefore a direct consequence of stability of $G_\theta(s)$ and $G_h(s)$, proved earlier in this section. □

Stability of $Q_\beta^{-1}(s)$:

Proof. In complex domain $Q_\beta^{-1}(s) = \frac{1}{1+A_\beta(s)}$ can be regarded as a negative feedback loop around $A_\beta(s)$. Since $A_\beta(s)$ is stable due to the stability of $Q_\beta(s)$, its Nyquist plot must not encircle the critical point -1. Here we prove that $|A_\beta(j\omega)| < 1$ holds at all frequencies. Since as β grows $A_\beta(s)$ converges to zero, it is sufficient to prove the above when $|A_\beta(j\omega)|$ obtains its largest values, i.e. for $\beta = 0$. Calculating $|A_0(j\omega)| = \sqrt{2g(\tau_\varepsilon\omega)}$ where $g(\tau_\varepsilon\omega) \doteq \frac{1-\cos\tau_\varepsilon\omega}{(\tau_\varepsilon\omega)^2 + (\tau_\varepsilon\eta)^2}$, we need to show that $|g(\tau_\varepsilon\omega)| < 1/2\ \forall\omega \geq 0$. The solutions of $g'(\tau_\varepsilon\omega) = 0$ satisfy $1 - \cos\tau_\varepsilon\omega = \frac{\sin(\tau_\varepsilon\omega)\left((\tau_\varepsilon\omega)^2 + (\tau_\varepsilon\eta)^2\right)}{2\tau_\varepsilon\omega}$ for $\omega > 0$. Substituting back to g yields $g(\tau_\varepsilon\omega) = \frac{1}{2}\mathrm{sinc}(\tau_\varepsilon\omega)$, which is clearly smaller than $\frac{1}{2}$ for all $\omega > 0$ ($g(0) = 0$ is a minimum). □

Stability of $\overline{Q}_\beta(s)G_\theta(s)$:

Proof. $\overline{Q}_\beta(s)$ is defined in (23) and $G_\theta(s)$ in (41). Substituting for $\overline{Q}_\beta(s)$ and $G_\theta(s)$ and using the relation $G_\theta(s)e^{\tau_\varepsilon\lambda(s)} = G_\Theta(s)$, where $\Theta = \theta - \tau_\varepsilon$, we obtain $\overline{Q}_\beta(s)G_\theta(s) = G_\theta(s) + G_h(s)G_\theta(s) - G_h(s)G_\Theta(s)$. Since stability of $G_\Theta(s)$ is essentially the same as of $G_\theta(s)$, $\overline{Q}_\beta(s)G_\theta(s)$ is stable due to stability of $G_\theta(s)$ and $G_h(s)$, proved earlier in this section. □

Stability of $1/\Delta_\mu(s)$:

Proof. Since the high frequency gain of $\frac{\mu_H s}{\mu_H s+1}$ is 1 for any μ_H, it will be sufficient to show that $|e^{-\tau\lambda(j\omega)}| < 1$ for all frequencies, where $\lambda(j\omega) = \beta\omega j - \omega^2$, provided $\beta > 0$. Defining $\beta\omega j - \omega^2 = re^{j\varphi}$, where $r = \omega\sqrt{\omega^2 + \beta^2}$ and $\varphi = \pi - \tan^{-1}\frac{\beta}{\omega}$, we obtain $\lambda(j\omega) = r^{\frac{1}{2}}e^{j\frac{\varphi}{2}}$ (considering only the positive branch of the square root for $\lambda(j\omega)$ to reduce to $j\omega$ for $\beta = 0$). Since $e^{j\frac{\varphi}{2}} = \cos\frac{\varphi}{2} + j\sin\frac{\varphi}{2}$, the real part of $e^{-\tau\lambda(j\omega)}$ is given by $e^{-\tau\cos\left(\frac{\pi}{2} - \frac{1}{2}\tan^{-1}\frac{\beta}{\omega}\right)} = e^{-\tau r^{1/2}\sin\left(\frac{1}{2}\tan^{-1}\frac{\beta}{\omega}\right)}$. Since $0 < \tan^{-1}\frac{\beta}{\omega} < \frac{\pi}{2}$ for $\beta > 0$ and thus $\sin\left(\frac{1}{2}\tan^{-1}\frac{\beta}{\omega}\right) > 0$, we obtain that $|e^{-\tau\lambda(j\omega)}| < 1$ for any $\beta > 0$. □

ACKNOWLEDGMENT

This work was supported in part by the MIT-Technion Program and in part by the National Science Foundation grants ECCS-1135815 and EFRI-1441301. We would like to thank Dr. Aranya Chakrabortty for his insightful comments and suggestions.

REFERENCES

[1] A. Chakrabortty, "Wide-area damping control of power systems using dynamic clustering and TCSC-based redesigns," *Smart Grid, IEEE Transactions on*, vol. 3, no. 3, pp. 1503–1514, 2012.

[2] X. Wu, F. Dörfler, and M. R. Jovanović, "Input-output analysis and decentralized optimal control of inter-area oscillations in power systems," *IEEE Transactions on Power Systems*, vol. 31, no. 3, pp. 2434–2444, 2016.

[3] F. Dörfler, M. R. Jovanović, M. Chertkov, and F. Bullo, "Sparsity-promoting optimal wide-area control of power networks," *IEEE Transactions on Power Systems*, vol. 29, no. 5, pp. 2281–2291, 2014.

[4] E. V. Larsen, J. J. Sanchez-Gasca, and J. H. Chow, "Concepts for design of FACTS controllers to damp power swings," *IEEE Transactions on power systems*, vol. 10, no. 2, pp. 948–956, 1995.

[5] U. Mhaskar and A. Kulkarni, "Power oscillation damping using FACTS devices: modal controllability, observability in local signals, and location of transfer function zeros," *Power Systems, IEEE Transactions on*, vol. 21, no. 1, pp. 285–294, 2006.

[6] R. Cresap and J. Hauer, "Emergence of a new swing mode in the western power system," *IEEE Transactions on Power Apparatus and Systems*, vol. 4, no. PAS-100, pp. 2037–2045, 1981.

[7] J. S. Thorp, C. E. Seyler, and A. G. Phadke, "Electromechanical wave propagation in large electric power systems," *Circuits and Systems I: Fundamental Theory and Applications, IEEE Transactions on*, vol. 45, no. 6, pp. 614–622, 1998.

[8] M. Parashar, J. S. Thorp, and C. E. Seyler, "Continuum modeling of electromechanical dynamics in large-scale power systems," *Circuits and Systems I: Regular Papers, IEEE Transactions on*, vol. 51, no. 9, pp. 1848–1858, 2004.

[9] D. F. Gayme and A. Chakrabortty, "Impact of wind farm placement on inter-area oscillations in large power systems," in *American Control Conference (ACC), 2012*. IEEE, 2012, pp. 3038–3043.

[10] S. Sahyoun, S. M. Djouadi, K. Tomsovic, and S. Lenhart, "Optimal distributed control for continuum power systems," in *2015 Proceedings of the Conference on Control and its Applications*. SIAM, 2015, pp. 416–422.

[11] B. C. Lesieutre, E. Scholtz, and G. C. Verghese, "Impedance matching controllers to extinguish electromechanical waves in power networks," in *Control Applications, 2002. Proceedings of the 2002 International Conference on*, vol. 1. IEEE, 2002, pp. 25–30.

[12] K. T. Magar, M. J. Balas, and D. F. Gayme, "Adaptive control of inter-area oscillations in wind-integrated power systems using distributed parameter control methods," in *American Control Conference (ACC), 2014*. IEEE, 2014, pp. 903–907.

[13] S.-J. Tsai, L. Zhang, A. G. Phadke, Y. Liu, M. R. Ingram, S. C. Bell, I. S. Grant, D. T. Bradshaw, D. Lubkeman, and L. Tang, "Frequency sensitivity and electromechanical propagation simulation study in large power systems," *Circuits and Systems I: Regular Papers, IEEE Transactions on*, vol. 54, no. 8, pp. 1819–1828, 2007.

[14] "https://www.youtube.com/watch?v=awvS4TtN77E."

[15] K. F. Graff, *Wave motion in elastic solids*. Courier Dover Publications, 1975.

[16] M. Krstic, B.-Z. Guo, A. Balogh, and A. Smyshlyaev, "Output-feedback stabilization of an unstable wave equation," *Automatica*, vol. 44, no. 1, pp. 63–74, 2008.

[17] B.-Z. Guo and H.-C. Zhou, "The active disturbance rejection control to stabilization for multi-dimensional wave equation with boundary control matched disturbance," *IEEE Transactions on Automatic Control*, vol. 60, no. 1, pp. 143–157, 2015.

[18] L. Sirota, Y. Halevi, and M. Krstic, "On the relationship between the absolute vibration suppression and back-stepping methods in control of the wave equation with possibly unstable boundary conditions," in *American Control Conference (ACC), 2016*. IEEE, 2016, pp. 6709–6714.

[19] R. Padhi and S. F. Ali, "An account of chronological developments in control of distributed parameter systems," *Annual Reviews in Control*, vol. 33, no. 1, pp. 59–68, 2009.

[20] L. Sirota and Y. Halevi, "Fractional order control of the two-dimensional wave equation," *Automatica*, vol. 59, pp. 152–163, 2015.

[21] ——, "Fractional order control of flexible structures governed by the damped wave equation," in *American Control Conference (ACC), 2015*. IEEE, 2015, pp. 565–570.

[22] Y. Halevi, "Control of flexible structures governed by the wave equation using infinite dimensional transfer functions," *Journal of dynamic systems, measurement, and control*, vol. 127, no. 4, pp. 579–588, 2005.

[23] L. Sirota and Y. Halevi, "Free response and absolute vibration suppression of second-order flexible structuresthe traveling wave approach," *Journal of Vibration and Acoustics*, vol. 132, no. 3, p. 031008, 2010.

[24] A. Chakrabortty and P. P. Khargonekar, "Introduction to wide-area control of power systems," in *American Control Conference (ACC), 2013*. IEEE, 2013, pp. 6758–6770.

[25] A. D. Del Rosso, C. A. Canizares, and V. M. Dona, "A study of tcsc controller design for power system stability improvement," *IEEE Transactions on Power Systems*, vol. 18, no. 4, pp. 1487–1496, 2003.

[26] L. Sirota and A. M. Annaswamy, "Spatially continuous modeling and control of swing dynamics in electric power grids," in *Internatioanl Federation of Automatic Control (IFAC) World Congress, 2017*. IFAC, 2017.

[27] P. M. Anderson and A. A. Fouad, *Power system control and stability*. John Wiley & Sons, 2008.

[28] P. W. Sauer, M. A. Pai, and J. H. Chow, *Power System Dynamics and Stability: With Synchrophasor Measurement and Power System Toolbox*. John Wiley & Sons, 2017.

[29] L. Sirota and Y. Halevi, "Extended d'Alembert solution of finite length second order flexible structures with damped boundaries," *Mechanical Systems and Signal Processing*, vol. 39, no. 1, pp. 47–58, 2013.

[30] ——, "The complete infinite series solution of systems governed by the wave equation with boundary damping," *Wave Motion*, vol. 51, no. 1, pp. 114–124, 2014.

[31] H. Bateman, A. Erdélyi, H. van Haeringen, and L. Kok, *Tables of integral transforms*. McGraw-Hill New York, 1954, vol. 1.

[32] M. Abramowitz and I. A. Stegun, *Handbook of mathematical functions: with formulas, graphs, and mathematical tables*. Courier Dover Publications, 2012.

[33] I. Avdonin, S. A. Avdonin, and S. A. Ivanov, *Families of exponentials: the method of moments in controllability problems for distributed parameter systems*. Cambridge University Press, 1995.

[34] J.-L. Lions, "Pointwise control for distributed systems," in *Control and estimation in distributed parameter systems*. SIAM, 1992, pp. 1–39.

[35] C. Castro, "Exact controllability of the 1-d wave equation from a moving interior point," *ESAIM: Control, Optimisation and Calculus of variations*, vol. 19, no. 1, pp. 301–316, 2013.

[36] L. Sirota and A. M. Annaswamy, "Active wave suppression in the interior of a one-domensional domain," *Automatica*, submitted.

[37] R. Dáger and E. Zuazua, *Wave propagation, observation and control in 1-D flexible multi-structures*. Springer Science & Business Media, 2006, vol. 50.

[38] S. Nicaise and J. Valein, "Stabilization of the wave equation on 1-D networks with a delay term in the nodal feedbacks," *NHM*, vol. 2, no. 3, pp. 425–479, 2007.

[39] J. Valein and E. Zuazua, "Stabilization of the wave equation on 1-D networks," *SIAM Journal on control and Optimization*, vol. 48, no. 4, pp. 2771–2797, 2009.

[40] E. Zuazua, "Control and stabilization of waves on 1-D networks," in *Modelling and optimisation of flows on networks*. Springer, 2013, pp. 463–493.

[41] O. Demir and H. Ozbay, "On reduced order modeling of flexible structures from frequency response data," in *Control Conference (ECC), 2014 European*. IEEE, 2014, pp. 1133–1138.

[42] Y. Chen and B. M. Vinagre, *Fractional-order systems and controls: fundamentals and applications*. Springer, 2010.

[43] B. Vinagre, I. Podlubny, A. Hernandez, and V. Feliu, "Some approximations of fractional order operators used in control theory and applications," *Fractional calculus and applied analysis*, vol. 3, no. 3, pp. 231–248, 2000.

[44] I. Podlubny, I. Petraš, B. M. Vinagre, P. O'leary, and L. Dorčák, "Analogue realizations of fractional-order controllers," *Nonlinear dynamics*, vol. 29, no. 1, pp. 281–296, 2002.

[45] D. Matignon, "Stability properties for generalized fractional differential systems," in *ESAIM: proceedings*, vol. 5. EDP Sciences, 1998, pp. 145–158.

[46] C. Bonnet and J. R. Partington, "Analysis of fractional delay systems of retarded and neutral type," *Automatica*, vol. 38, no. 7, pp. 1133–1138, 2002.

[47] ——, "Stabilization of some fractional delay systems of neutral type," *Automatica*, vol. 43, no. 12, pp. 2047–2053, 2007.

[48] A. R. Fioravanti, C. Bonnet, H. Özbay, and S.-I. Niculescu, "A numerical method for stability windows and unstable root-locus calculation for linear fractional time-delay systems," *Automatica*, vol. 48, no. 11, pp. 2824–2830, 2012.

Lea Sirota Biography text here.

Anuradha M. Annaswamy Biography text here.